GPS Solutions (2022) 26:97
https://doi.org/10.1007/s10291-022-01280-w

ORIGINAL ARTICLE

Scalar and vector tracking loop simulation based on a uniform semi-analytic model and robustness analysis in multipath/NLOS situations

Qiongqiong Jia[1] · **Li-Ta Hsu**[2] · **Renbiao Wu**[1]

Received: 29 December 2020 / Accepted: 30 May 2022 / Published online: 27 June 2022

Abstract
A semi-analytic model is proposed to efficiently analyze and compare the performance of both the scalar tracking loop (STL) and the vector tracking loop (VTL) in different operating situations. The quality of each satellite signal, including multipath and none-line-of-sight (NLOS) propagation problems, can be incorporated into the proposed model for different configurations of deteriorated situations. Theoretical analysis of multipath and NLOS induced bias to the VTL and STL is given, including the bias envelop, from which a conclusion is obtained that the VTL performance is not better than the STL in certain multipath situations. The results from the semi-analytic model verify the theoretical analysis. The effectiveness of the proposed model is verified by a comparison with the results from simulated NLOS data processed by a software-defined radio receiver.

Keywords GNSS · Multipath · Non-line-of-sight (NLOS) propagation · Scalar tracking loop (STL) · Vector tracking loop (VTL)

Introduction

The vector tracking loop (VTL), which uses internal aiding among the tracking channels (Spilker 1996), achieves a more robust performance compared to the classic scalar tracking loop (STL) under degraded conditions. However, the internal aiding of the VTL also has some drawbacks, e.g., the tracking bias caused by multipath/Non-line-of-sight (NLOS) in one tracking channel may corrupt other channels, which is termed the bias propagation phenomenon of a VTL (Xu and Hsu 2019; Zhao et al. 2011).

✉ Qiongqiong Jia
qiongjiawei@163.com

✉ Renbiao Wu
rbwu@cauc.edu.cn

Li-Ta Hsu
lt.hsu@polyu.edu.hk

[1] Tianjin Key Lab for Advanced Signal Processing, Civil Aviation University of China, Tianjin, China

[2] Interdisciplinary Division of Aeronautical and Aviation Engineering, The Hong Kong Polytechnic University, Hong Kong SAR, China

The tracking and navigation performance of STLs and VTLs are commonly compared by processing data collected in a degraded environment (Zhao et al. 2011; Hsu et al. 2015). However, a field test is confronted with many uncontrollable factors that limit its flexibility. Additionally, non-real-time data processing is time-consuming. Analytic methods, such as the noise bandwidth method (Bhattacharyya and Demoz 2010; Bhattacharyya 2018), and the carrier to noise power density ratio (C/N0) threshold (Lashley et al. 2009; Hsu et al. 2015) are also used to illustrate the performance of the VTL. However, the nonlinear nature of the VTL is not considered in the analytic method; thus, it cannot reflect the actual performance and cannot provide the tracking and navigation error evaluation.

Semi-analytic techniques, with the advantages of flexibility, computation efficiency, and retention of the nonlinear characteristics of the receiver, are proposed for STL and VTL performance analysis in Borio et al. (2011) and Luo et al. (2019), respectively. However, the different structures of the two semi-analytic methods make it unfair to compare the performance of the STL and VTL. We propose a new semi-analytic model with a uniform framework for both STLs and VTLs in Jia and Wu (2020) to overcome the above limitations. The quality of each satellite signal,

including multipath and NLOS, can be incorporated into our proposed model for different deteriorated situations. We extend our previous work by robustness analysis of the two receiver structures in multipath and NLOS reception environments, including analysis of the bias envelope and bias propagation phenomenon in a VTL. Furthermore, the proposed semi-analytic model results are given to verify the theoretical analysis. The tracking results from the proposed model are also compared with simulated NLOS data that is processed by a software-defined radio (SDR) receiver. This helps in verifying the effectiveness of the proposed semi-analytic model.

First, the GNSS principles are briefly reviewed. Second, the proposed semi-analytic model is described. Third, the robustness of STLs and VTLs to multipath and NLOS is discussed, and experimental results are presented. Finally, some conclusions and future work are given.

We will use the following notations:

$\mathbf{a}/\mathbf{A}$: bold face lower case/ capital letters denote column vectors/ matrices.
a_k^m: the subscript k denotes the epoch index, while the superscript m stands for the satellite index.
a^-, a^+: the superscript "−" denotes the a priori prediction, while "+" denotes the corresponding posterior estimation after filtering.
$\hat{a}$: denotes the estimation of a.
δa: denotes the residual of a, which is defined as $\delta a = a - a^-$, or $\delta a = a - \hat{a}$.
$(\bullet)^{\mathrm{T}}$: is the transpose operator.
$f^{-1}(\cdot)$: is the inversion function of $f(\cdot)$.

Two receiver structures: STL and VTL

Basic principles of GNSS navigation are given first, then the difference between STLs and VTLs is discussed. To provide a fair comparison between STL and VTL, we choose the EKF as the navigation solution approach for both.

From measurements to the navigation solution

Define $\mathbf{x} = \left[\mathbf{p}, \mathbf{v}, ct_b, c\dot{t}_b\right]^{\mathrm{T}}$ as the user state, where $\mathbf{p}$ and $\mathbf{v}$ stand for the 3-Dimensional (3D) user position and user velocity in the earth-centered earth-fixed (ECEF) coordinate system, respectively. The variables t_b and $\dot{t}_b$ denote the user clock bias and drift, where c is the speed of light.

The pseudorange and pseudorange rate from all the tracking channels are written as a vector $\mathbf{y}_k = \left[\rho_k^1, \rho_k^2, \ldots, \rho_k^M, \dot{\rho}_k^1, \dot{\rho}_k^2, \ldots, \dot{\rho}_k^M\right]^{\mathrm{T}}$. The relation between the measurements and the user state can be written as (Kaplan and Hegarty 2006)

$$\mathbf{y}_k = h\left(\mathbf{x}_k\right) + \mathbf{n}_k \tag{1}$$

where $h(\cdot)$ stands for the observation function, and $\mathbf{n}_k$ denotes the noise vector. The state vector $\mathbf{x}_k$ is unknown and to be estimated by the measurements. Actually, the state vector of the satellites should be included in the observation function, which is omitted here for concise expression.

With a priori user state predication $\mathbf{x}_k^-$ from the EKF, the first-order Taylor series expansion of (1) is given below (Lesouple et al. 2019)

$$\mathbf{y}_k \approx h\left(\mathbf{x}_k^-\right) + \mathbf{H}_k \delta\mathbf{x}_k + \mathbf{n}_k \tag{2}$$

where $\mathbf{H}_k$ is the Jacobian of $h(\cdot)$ (Zhao et al. 2011). The measurement residual is given as

$$\mathbf{z}_k = \mathbf{y}_k - \mathbf{y}_k^- = \mathbf{H}_k \delta\mathbf{x}_k + \mathbf{n}_k \tag{3}$$

which is sent to the EKF to obtain a posterior estimation $\delta\mathbf{x}_k^+$ (Luo et al. 2019; Zhao et al. 2011). The a posteriori user state estimate is updated by

$$\mathbf{x}_k^+ = \mathbf{x}_k^- + \delta\mathbf{x}_k^+ \tag{4}$$

where $\mathbf{x}_k^+$ also corresponds to the navigation solution.

Comparison between STL and VTL

The satellite transmitted signals reach the user receiver with a time delay, which is the time of propagation $\mathbf{t}_{\mathrm{op},k}$. It is the difference between the time of transmission and the time of reception $\mathbf{t}_{\mathrm{or},k}$. The former is measured from the received signal, while the latter is read from the receiver. The instantaneous code phase $\boldsymbol{\upsilon}_k$ can be expressed as the sum of full code cycles and fractional cycle, i.e., $\boldsymbol{\upsilon}_k = \mathbf{L}_k + \boldsymbol{\kappa}_k$, the measuring unit of which is code cycle. Since the code cycle T_{code} is fixed for each kind of the pseudo random code, the code phase can also be represented as a time quantity $\boldsymbol{\tau}_k = \boldsymbol{\upsilon}_k T_{\mathrm{code}}$, which is a measure of the transmission time.

The code phase $\boldsymbol{\tau}_k$ in seconds, the Doppler $\mathbf{f}_{dk}$ in Hz and the carrier phase $\boldsymbol{\varphi}_k$ in rad/s are termed the synchronization parameters. The m-th elements of the vectors $\boldsymbol{\tau}_k, \mathbf{f}_{dk}, \boldsymbol{\varphi}_k$ are the corresponding parameters of the m-th satellite signal. The process of making GNSS measurements involves controlling the code and carrier generators using their Numerically Controlled Oscillator (NCO). This permits the receiver to generate local signals that match the received signals as closely as possible. Thus, the synchronization parameters of the replica $\left[\hat{\boldsymbol{\tau}}_k^{\mathrm{T}}, \hat{\mathbf{f}}_{dk}^{\mathrm{T}}\right]^{\mathrm{T}}$ follow the ones of the received signal $\left[\boldsymbol{\tau}_k^{\mathrm{T}}, \mathbf{f}_{dk}^{\mathrm{T}}\right]^{\mathrm{T}}$. The misalignment between the locally generated replica and the actual received signal is the synchronization parameter residuals $\left[\delta\boldsymbol{\tau}_k^{\mathrm{T}}, \delta\mathbf{f}_{dk}^{\mathrm{T}}\right]^{\mathrm{T}} = \left[\boldsymbol{\tau}_k^{\mathrm{T}}, \mathbf{f}_{dk}^{\mathrm{T}}\right]^{\mathrm{T}} - \left[\hat{\boldsymbol{\tau}}_k^{\mathrm{T}}, \hat{\mathbf{f}}_{dk}^{\mathrm{T}}\right]^{\mathrm{T}}$, which are usually sensed by the discriminators.

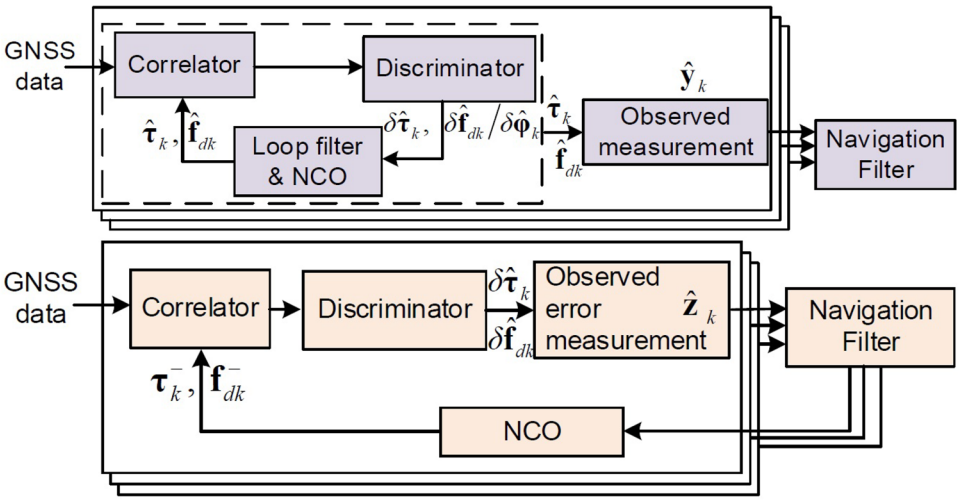

Fig. 1 Conventional receiver block diagram, where the data with satellite signals are sent to each of the tracking channels, shown as the overlapped solid rectangle boxes. The dashed box denotes DLL in STL. The measurements from the tracking channels are fed to the navigation filter. The STL is shown on the top panel, while the VTL is on the bottom

The STL and VTL receiver structures are shown in Fig. 1. It is noted that the STL tracking channels work independently, and each of them outputs its own measurement. While for the VTL, the tracking channels are coupled together by the feeding from the navigation solution. There are various kinds of VTL structures, e.g., the vector delay lock loop (VDLL) (Hsu et al. 2015), which replaces the conventional delay lock loop (DLL) but retains the conventional individual frequency lock loop (FLL) or individual phase lock loop (PLL), the vector frequency lock loop (VFLL), which replaces only the conventional FLL, and the vector phase lock loop (VPLL) which replaces only the individual PLL (Lashley 2009). The vector delay and frequency lock loop (VDFLL), which replace both the individual DLL and FLL, are considered in this work (Zhao et al. 2011).

An STL receiver contains a DLL, regardless of whether it contains a single PLL, a single FLL, or both, depending on the type of receiver architecture adopted. For the STL, its measurements are generally made by examining the state of the locally generated signals at a regular rate, which is defined by a hardware counter. The hardware counter outputs pulses to latch the state of all the NCOs that are tracking satellites. The cumulative count of the hardware counter is the 'time-of-reception' $\mathbf{t}_{\mathrm{or},k}$. The latched code phases $\hat{\boldsymbol{\tau}}_k$ from each locally generated replica are the estimated 'times-of-transmission' from each satellite. The code phases are measured depending on the timing of the time-of-reception hardware counter. The 'time-of-propagation' is obtained by comparing the signal transmission time with the local receiver time, with which the pseudorange is calculated by

$$\hat{\boldsymbol{\rho}}_k = \mathrm{c} \times \left(\mathbf{t}_{\mathrm{or},k} - \hat{\boldsymbol{\tau}}_k\right) = g_1\left(\hat{\boldsymbol{\tau}}_k\right) \tag{5}$$

Since $\mathbf{t}_{\mathrm{or},k}$ can be read from the receiver directly, the measurements are expressed as a function of the signal transmission time $\hat{\boldsymbol{\tau}}_k$, as the second part of (5) (Kaplan and Hegarty 2006).

The carrier frequency of the STL can be measured by taking the NCO value that is used to control the FLL or PLL and then converting that to Hz. Then the pseudorange rate vector can be obtained by

$$\hat{\dot{\boldsymbol{\rho}}}_k = \lambda_{\mathrm{carr}} \hat{\mathbf{f}}_{dk} = g_2\left(\hat{\mathbf{f}}_{dk}\right) \tag{6}$$

where λ_{carr} denotes the wavelength of the carrier. The inputs to the FLL or PLL are generally a phase or frequency discriminator. Since the discriminator output contains much noise, the purpose of the loop filter is to reduce the noise effect.

Equations (5) and (6) are written in a compact form below for simplicity

$$\hat{\mathbf{y}}_k = \begin{bmatrix} g_1\left(\hat{\boldsymbol{\tau}}_k\right) \\ g_2\left(\hat{\mathbf{f}}_{dk}\right) \end{bmatrix} = g\left(\begin{bmatrix} \hat{\boldsymbol{\tau}}_k \\ \hat{\mathbf{f}}_{dk} \end{bmatrix}\right) \tag{7}$$

The defined function $g(\cdot)$ maps each of the estimated synchronization parameters in vector $\left[\hat{\boldsymbol{\tau}}_k^{\mathrm{T}}, \hat{\mathbf{f}}_{dk}^{\mathrm{T}}\right]^{\mathrm{T}}$ to one measurement in vector $\hat{\mathbf{y}}_k$. Refer to (7), the relation between the true synchronization parameters and the measurements is

$$\mathbf{y}_k = g\left(\begin{bmatrix} \boldsymbol{\tau}_k \\ \mathbf{f}_{dk} \end{bmatrix}\right) \tag{8}$$

It is noted from (1) and (7) that there is a one-to-one relationship between the user state, the measurements, and the synchronization parameters under a given user-satellites geometry.

By using the relation (1), the prior prediction of the measurement can be obtained by

$$\mathbf{y}_k^- = h\left(\mathbf{x}_k^-\right) \tag{9}$$

Then the estimated measurement residual of the STL is given by

$$\hat{\mathbf{z}}_k = \hat{\mathbf{y}}_k - \mathbf{y}_k^- \tag{10}$$

The observed measurement (7) is the output of the tracking channels, while the prior prediction of the measurement (9) is implemented in the navigation module of the STL. These two parts work independently in STLs.

The internal aiding of the VTL is based on the relation between the predicated synchronization parameters $\boldsymbol{\tau}_k^-, \mathbf{f}_{dk}^-$ for the local replica and the predicated user state as below

$$\begin{bmatrix} \boldsymbol{\tau}_k^- \\ \mathbf{f}_{dk}^- \end{bmatrix} = g^{-1}\left(h\left(\mathbf{x}_k^-\right)\right) \tag{11}$$

Specifically, the a prior user state increment $\Delta\mathbf{x}_k^- = \mathbf{x}_k^- - \mathbf{x}_{k-1}^+$ is used to calculate the increment of the synchronization parameters

$$\begin{bmatrix} \Delta\boldsymbol{\tau}_k^- \\ \Delta\mathbf{f}_{dk}^- \end{bmatrix} = g^{-1}\left(\mathbf{H}_k \Delta\mathbf{x}_k^-\right) \tag{12}$$

which are sent to the NCOs to obtain $\boldsymbol{\tau}_k^-, \mathbf{f}_{dk}^-$.

By inserting (8) into (3), the VTL true measurement residual can be reformulated as

$$\mathbf{z}_k = g\left(\begin{bmatrix} \boldsymbol{\tau}_k \\ \mathbf{f}_{dk} \end{bmatrix}\right) - g\left(\begin{bmatrix} \boldsymbol{\tau}_k^- \\ \mathbf{f}_{dk}^- \end{bmatrix}\right) \tag{13}$$

By inserting (5) and (6) into (13), we have

$$\mathbf{z}_k = \begin{bmatrix} \overline{g}_1\left(\delta\boldsymbol{\tau}_k\right) \\ g_2\left(\delta\mathbf{f}_{dk}\right) \end{bmatrix} = \overline{g}\left(\begin{bmatrix} \delta\boldsymbol{\tau}_k \\ \delta\mathbf{f}_{dk} \end{bmatrix}\right) \tag{14}$$

A new function is defined as $\overline{g}_1\left(\delta\boldsymbol{\tau}_k\right) = \mathrm{c} \times \delta\boldsymbol{\tau}_k$ in the second equation of (14), and the relation is further defined as a $\overline{g}(\cdot)$ function in the third equation for simplicity. Since the discriminator output is the estimation of the synchronization parameter residual, the VTL measurements are generally made by examining the discriminator outputs at a regular rate, then calculating its measurement residuals (Luo et al. 2019; Zhao et al. 2011)

$$\hat{\mathbf{z}}_k = \overline{g}\left(\begin{bmatrix} \delta\hat{\boldsymbol{\tau}}_k \\ \delta\hat{\mathbf{f}}_{dk} \end{bmatrix}\right) \tag{15}$$

It should be pointed out that a local filter is included after each discriminator to decrease the noise effect in some of the VTL implementations (Hsu et al. 2015), while the others do not contain a local filter (Zhao et al. 2011). The one without the local filter is considered in this work.

Proposed semi-analytic model

The block diagrams of the proposed uniform framework semi-analytic models for an STL and VTL are shown in Fig. 2; both include three key modules that are shown in different colors. The details of the proposed semi-analytic are given below.

Parameters setting module

The satellite parameter setting includes the number of satellites, the $\mathrm{C/N_0}$ of each satellite signal, and the geometric distribution. The satellite motion can be modeled, use a real trajectory from the ephemeris, or be assumed stationary if a limited simulation time is considered for simplicity.

The operation mode of the tracking loop, e.g., PLL only mode or FLL assisted PLL mode, etc.; the parameters of the loop filters, such as the loop order, the bandwidth of the loop filter, the initialization parameters of the NCO can also be set in advance. Initialization parameters of the EKF, the initial synchronization parameters $\boldsymbol{\tau}_0, \mathbf{f}_{d0}, \boldsymbol{\varphi}_0$ and the covariance matrix of the process noise $\mathbf{Q}$ can also be set in this module.

Analytic module based on parameter increment

With an initial user state $\mathbf{x}_0$, the user state at epoch k is calculated by the user motion model as below

$$\mathbf{x}_k = \mathbf{F}_{k-1,k}\mathbf{x}_{k-1} + \mathbf{w}_k \tag{16}$$

where $\mathbf{w}_k$ represents the random perturbation on the user state, which is termed as the process noise. The process noise $\mathbf{w}_k$ can be generated by the given statistic characteristic that is described by its covariance matrix $\mathbf{Q}$ (Luo et al. 2019; Xu and Hsu 2019). We use the parameters increment to calculate the true synchronization parameters. The user state increment from epoch $k-1$ to k is denoted as $\Delta\mathbf{x}_{k-1,k}$, with which the user synchronization parameters of the subsequent epochs are calculated by

$$\begin{bmatrix} \boldsymbol{\tau}_k \\ \mathbf{f}_{dk} \end{bmatrix} = \begin{bmatrix} \boldsymbol{\tau}_{k-1} \\ \mathbf{f}_{d(k-1)} \end{bmatrix} + \overline{g}^{-1}\left(\mathbf{H}_k\left(\Delta\mathbf{x}_{k-1,k}\right)\right) \tag{17}$$

The carrier phase is related to the carrier frequency by

$$\boldsymbol{\varphi}_k = \mathrm{rem}\left(2\pi\mathbf{f}_{d0}t + \boldsymbol{\varphi}_0, 2\pi\right) \tag{18}$$

where t is the elapsed simulation time and $\boldsymbol{\varphi}_0$ denotes the initial carrier phase. The operator $\mathrm{rem}(\cdot)$ denotes the remainder operation. Considering the random perturbation $\mathbf{w}_k$ on the user state in (16), the Doppler frequency will not be a constant. Therefore, equation (18) does not hold anymore.

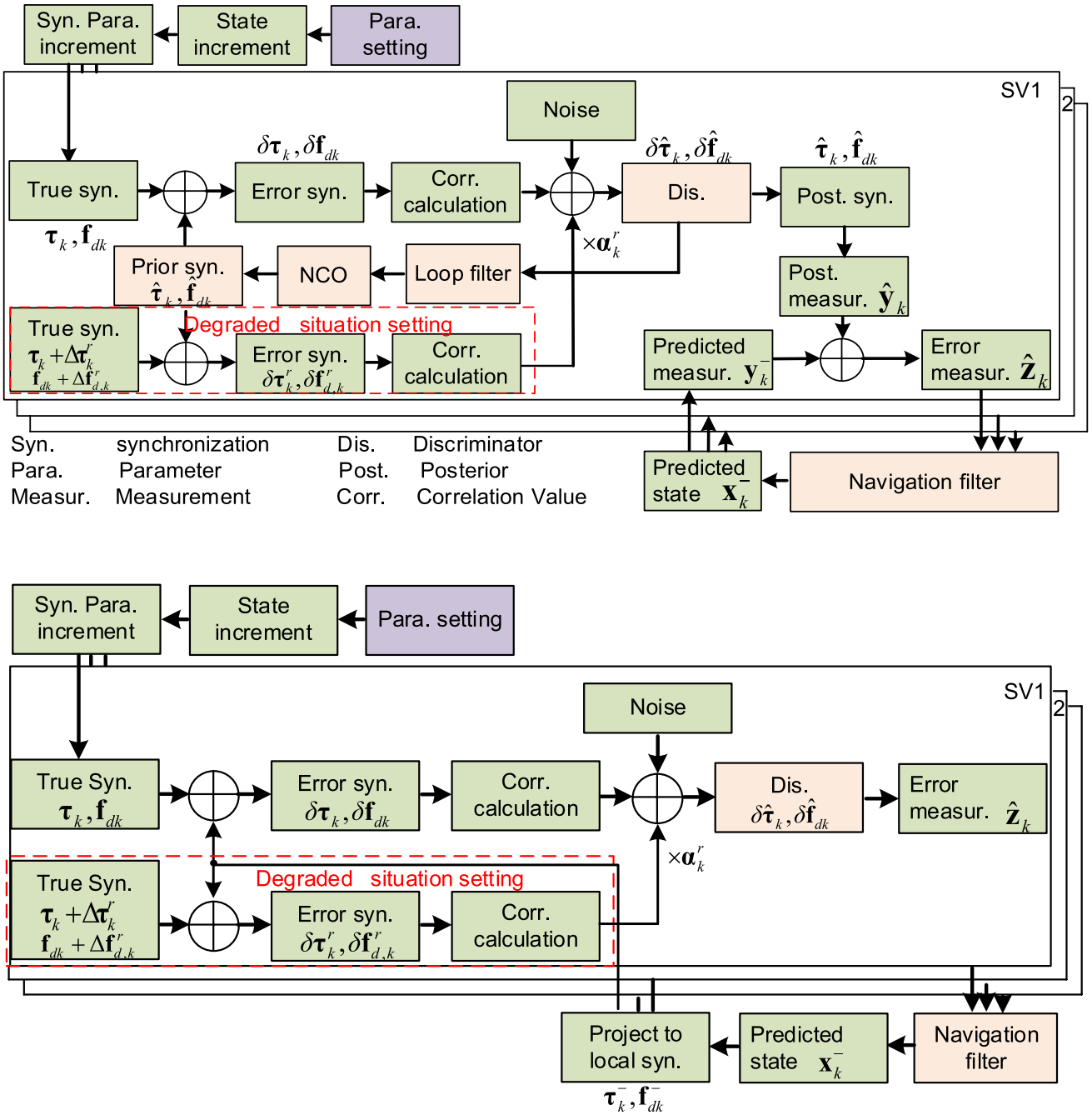

Fig. 2 Block diagram of the proposed semi-analytic model. The simulation parameters setting modules are in purple boxes, the analytic modules are in the green boxes and the numerical simulation modules are in the orange boxes, and the boxes in the dashed rectangles are for the situation setting, e.g., multipath or NLOS reception. The STL is shown on the top panel, while the VTL is on the bottom

Since the pre-detection integration period T_{coh} is very short, the constant Doppler frequency can be assumed in each of the pre-detection integration periods, the following relation can be used to obtain the carrier phase of each epoch

$$\boldsymbol{\varphi}_k = \text{rem}\left(2\pi \mathbf{f}_{d(k-1)} T_{coh} + \boldsymbol{\varphi}_{k-1}, 2\pi\right) \tag{19}$$

The true values of the synchronization parameters stand for the ones carried by the received signals. The synchronization parameter residuals $\left[\delta\boldsymbol{\tau}_k^{\mathrm{T}}, \delta\mathbf{f}_{dk}^{\mathrm{T}}\right]^{\mathrm{T}}$ and the carrier phase residual $\delta\boldsymbol{\varphi}_k$ stand for the difference between the true parameters $\boldsymbol{\tau}_k, \mathbf{f}_{dk}, \boldsymbol{\varphi}_k$ of the incoming signals and predicated ones of the local replica $\boldsymbol{\tau}_k^-, \mathbf{f}_{dk}^-, \boldsymbol{\varphi}_k^-$ in the VTL or the estimated ones $\hat{\boldsymbol{\tau}}_k, \hat{\mathbf{f}}_{dk}, \hat{\boldsymbol{\varphi}}_k$ in the STL.

In the proposed model, the true user state, the true synchronization parameters, and the synchronization parameter residuals for the STL and VTL are calculated in the same way as given above so that the proposed model can provide a performance comparison between STL and VTL fairly.

For an STL, the estimated ones $\hat{\boldsymbol{\tau}}_k, \hat{\mathbf{f}}_{dk}$ and $\hat{\boldsymbol{\varphi}}_k$ are obtained from the loop filter and the NCO (Kaplan and Hegarty 2006), which belongs to the numerical simulation module. For the VTL, the prior estimates of the synchronization parameters are calculated by the below parameters increment model

$$\begin{bmatrix} \boldsymbol{\tau}_k^- \\ \mathbf{f}_{dk}^- \end{bmatrix} \approx \begin{bmatrix} \boldsymbol{\tau}_k \\ \mathbf{f}_{dk} \end{bmatrix} + \overline{g}^{-1}\left(\mathbf{H}_k\left(\mathbf{x}_k^- - \mathbf{x}_k\right)\right) \tag{20}$$

Thus the true synchronization parameters residuals for the VTL can be written as

$$\begin{bmatrix} \delta\boldsymbol{\tau}_k \\ \delta\mathbf{f}_{dk} \end{bmatrix} = \overline{g}^{-1}\left(\mathbf{H}_k\left(\mathbf{x}_k - \mathbf{x}_k^-\right)\right) \tag{21}$$

Since a PLL is not necessary in a VTL, the error carrier phase cannot be obtained for the lack of the prior estimation of the carrier phase $\boldsymbol{\varphi}_k^-$. The true carrier phase residual in a VTL can be calculated by the trapezoidal integration rule below (Luo et al. 2019)

$$\delta\boldsymbol{\varphi}_k = \delta\boldsymbol{\varphi}_{k-1} + 0.5T_{\mathrm{coh}}\left(\delta\mathbf{f}_{d(k-1)} + \delta\mathbf{f}_{dk}\right) \tag{22}$$

with the obtained synchronization parameter residuals, the mixing and correlation process are realized analytically by

$$I_k^m + jQ_k^m = A_k^m R\left(\delta\tau_k^m\right)\mathrm{sinc}\left(\delta f_{dk}^m \times T_{coh}\right)\exp\left(j \times \delta\varphi_k^m\right) + \eta_k^m \tag{23}$$

where I_k^m and Q_k^m denote the correlation values from the in-phase and quadrature branches of the m-th tracking channels. The function $R(\cdot)$ stands for the auto-correlation function of the code, and A_k^m stands for the amplitude of the correlation value. The noise term at the correlator level is denoted as η_k^m (Borio et al. 2011). The mixing and correlations processes are the same for both the STL and VTL.

The measurement residuals of the STL and VTL are obtained in different ways. Based on (2), the prior measurement estimation is given by

$$\mathbf{y}_k^- = h\left(\mathbf{x}_k^-\right) \approx h\left(\mathbf{x}_k\right) + \mathbf{H}_k\left(\mathbf{x}_k^- - \mathbf{x}_k\right) \tag{24}$$

It's not convenient to obtain the first term in (24); hence it is further reformulated as

$$\mathbf{y}_k^- \approx g\left(\begin{bmatrix} \boldsymbol{\tau}_k \\ \mathbf{f}_{d,k} \end{bmatrix}\right) + \mathbf{H}_k\left(\mathbf{x}_k^- - \mathbf{x}_k\right) \tag{25}$$

The measurement residuals $\hat{\mathbf{z}}_k$ can be obtained by inserting (7) and (25) into (10) as follows

$$\hat{\mathbf{z}}_k = \overline{g}\left(\begin{bmatrix} \hat{\boldsymbol{\tau}}_k - \boldsymbol{\tau}_k \\ \hat{\mathbf{f}}_{d,k} - \mathbf{f}_{d,k} \end{bmatrix}\right) - \mathbf{H}_k\left(\mathbf{x}_k^- - \mathbf{x}_k\right) \tag{26}$$

Equation (26) notes that the measurement residuals can be analytically calculated from the obtained parameters increment value.

For the VTL, the measurement residuals $\hat{\mathbf{z}}_k$ can be directly obtained from the discriminator output by (15). The obtained measurement residuals are then sent to the EKF to update the navigation solution.

Numerical simulation module

The correlation values from (23) are sent to the discriminators. In the semi-analytic STL model, the loop filters and the NCOs are also required, from which the estimates of the synchronization parameters $\hat{\boldsymbol{\tau}}_k, \hat{\mathbf{f}}_{dk}$ and $\hat{\boldsymbol{\varphi}}_k$ can be obtained. Then the true synchronization parameter residuals can be calculated.

In the proposed semi-analytic VTL model, the prior estimation of the synchronization parameters $\boldsymbol{\tau}_k^-, \mathbf{f}_{dk}^-$ can be calculated from (20) analytically, then the synchronization parameter residuals $\delta\boldsymbol{\tau}_k, \delta\mathbf{f}_{d,k}$ and $\delta\boldsymbol{\varphi}_k$ can be obtained. Therefore, the NCOs are not required in the proposed semi-analytic VTL model.

With the measurement residuals from the analytic module, the user state residual estimates $\delta\mathbf{x}_k^+$ can be obtained from the navigation filter, and further the user state estimate $\mathbf{x}_k^+$ can be calculated using (4). The difference between the STL and the VTL in the proposed semi-analytic model is summarized in Table 1.

Deteriorated situation setting

To evaluate the tracking and navigation performance of the STL and the VTL in a degraded environment, we incorporate the test case configuration module in the proposed model, shown as the dashed red box in Fig. 2. In the proposed model, the synchronization parameters difference between the reflected signal and the LOS signal, i.e., $\Delta\boldsymbol{\tau}_k^r$, $\Delta\mathbf{f}_{d,k}^r$, $\Delta\boldsymbol{\varphi}_k^r$ and the relative amplitude $\boldsymbol{\alpha}_k^r$, are the input of the test situation setting module. The elements of $\Delta\boldsymbol{\tau}_k^r$, $\Delta\mathbf{f}_{d,k}^r$, $\Delta\boldsymbol{\varphi}_k^r$ and $\boldsymbol{\alpha}_k^r$ are nonzero only for the channels contaminated by multipath or NLOS (Zhang et al. 2020). The synchronization parameter residuals of the reflected signal are given by

$$\begin{bmatrix} \delta\boldsymbol{\tau}_k^r \\ \delta\mathbf{f}_{d,k}^r \end{bmatrix} = \begin{bmatrix} \delta\boldsymbol{\tau}_k \\ \delta\mathbf{f}_{d,k} \end{bmatrix} + \begin{bmatrix} \Delta\boldsymbol{\tau}_k^r \\ \Delta\mathbf{f}_{d,k}^r \end{bmatrix} \tag{27}$$

Table 1 Difference between STL and VTL in the proposed semi-analytic model

	STL	VTL
$\left[\boldsymbol{\tau}_k^-, \mathbf{f}_{d,k}^-\right]$	DLL and PLL/FLL	$\left[\boldsymbol{\tau}_k^-, \mathbf{f}_{d,k}^-\right] \approx \left[\boldsymbol{\tau}_k, \mathbf{f}_{d,k}\right] + g^{-1}\left(\mathbf{H}\left(\mathbf{x}_k^- - \mathbf{x}_k\right)\right)$
$\boldsymbol{\varphi}_k^-$	PLL	Not required
$\delta\boldsymbol{\varphi}_k$	$\delta\boldsymbol{\varphi}_k = \boldsymbol{\varphi}_k - \boldsymbol{\varphi}_k^-$	$\delta\boldsymbol{\varphi}_k = \delta\boldsymbol{\varphi}_{k-1} + 0.5T_{coh}\left(\delta\mathbf{f}_{d,k-1} + \delta\mathbf{f}_{d,k}\right)$
$\left[\hat{\boldsymbol{\tau}}_k, \hat{\mathbf{f}}_{dk}\right]$	Equal to $\left[\boldsymbol{\tau}_k^-, \mathbf{f}_{d,k}^-\right]$	Not required
$\hat{\boldsymbol{\varphi}}_k$	Equal to $\boldsymbol{\varphi}_k^-$	Not required
$\hat{\mathbf{z}}_k$	$\hat{\mathbf{z}}_k = g\left(\hat{\boldsymbol{\tau}}_k - \boldsymbol{\tau}_k, \hat{\mathbf{f}}_{d,k} - \mathbf{f}_{d,k}\right) - \mathbf{H}\left(\mathbf{x}_k^- - \mathbf{x}_k\right)\hat{\mathbf{z}}_k = g\left(\delta\hat{\boldsymbol{\tau}}_k, \delta\hat{\mathbf{f}}_{d,k}\right)$	

The first column contains the parameters to be calculated in the proposed semi-analytic models. The second and the third columns show how to calculate the parameters in the STL and the VTL, respectively

and

$$\delta\boldsymbol{\varphi}_k^r = \delta\boldsymbol{\varphi}_k + \Delta\boldsymbol{\varphi}_k^r \tag{28}$$

Then the correlation value of the reflected signal is calculated by (23), the amplitude of the correlation value is controlled by $\boldsymbol{\alpha}_k^r$. In a multipath situation, the correlation value is the LOS plus the reflected one (Jia et al. 2017), while in an NLOS situation, only the reflected correlation value is left (Hsu 2018).

Robustness of STL and VTL in Multipath/NLOS situations

The robustness of the two receiver structures in multipath and NLOS situations is discussed below. First, the multipath and NLOS induced bias are illustrated, then the tracking bias phenomenon is discussed theoretically.

Multipath and NLOS induced bias

Figure 3 is used to illustrate the multipath/NLOS-induced tracking bias to the STL and VTL. The STL adjusts the synchronization parameters of the local replica so that its discriminator output is equal to zero (Nee 1992). Therefore, the local replica position of the STL should ensure that both the early and late correlation values, shown as the red crosses on the combined correlation curve, are equal, and the value of the affected discriminator curve equals zero. Based on this fact, the position of the local replica is given as the bold black line in Fig. 3; it is noted that a horizontal offset between the top panel and the bottom panel appears. The multipath induced bias to the STL is the horizontal deviation of the affected discriminator curves from the ideal ones on the left and middle panels, which is denoted as b_s, as discussed in Kaplan and Hegarty (2006).

For the VTL, the position of the local replica depends on the multipath/NLOS-affected navigation solution. Considering the internal aiding of the VTL, one can assume that the channel with multipath reception is less affected compared to the STL. Therefore, the local replica of the VTL given in Fig. 3 is less deviated from the vertical axis than the local replica of the STL. The deviation of this local replica from the vertical axis on the top panel is denoted as b_{v1}. The discriminator output is the intersection of the local replica and the multipath-affected discriminator curve, which is denoted as b_{v2}. In the ideal case without multipath, $b_{v2} = b_{v1}$, while in the appearance of multipath $b_{v2} \neq b_{v1}$. The difference $b_v = b_{v2} - b_{v1}$ is actually the multipath-induced bias to the VTL. The VTL local replica shown in Fig. 3 is merely a schematic one; the true value depends on the specific value of the affected navigation solution.

Multipath induced bias envelopes are given in Fig. 4, with α denoting the amplitude ratio of the reflected signal to the LOS one. The horizontal axis denotes the relative delay in chips of the reflected signal to the direct one, while the vertical axis denotes the multipath induced tracking bias. The curves above the horizontal axis are the results of constructive multipath where the phase difference between the LOS signal and the reflected one is fixed to zero. The curves below the horizontal axis correspond to the destructive multipath where the phase difference is π. The VTL plots are obtained by calculating the b_v as the relative delay of the reflected signal varies. Specifically, suppose the delay of the LOS signal is zero; then, with a given relative delay of the reflected signal and a preset the local replica offset b_{v1}, the early and late correlator outputs are calculated analytically. The outputs of the correlators are then sent to the discriminator to obtain the b_{v2}. Finally, the multipath induced bias is calculated by $b_v = b_{v2} - b_{v1}$. For each relative code delay of the reflected signal, repeat the above procedure to obtain a complete curve. The local replica offset of a VTL is controlled by the navigation solutions and the geometric distribution of the satellites, etc. Therefore, multiple VTL plots correspond to different offsets are shown in Fig. 4. It should be pointed out that each of the VTL plots only indicates the multipath induced

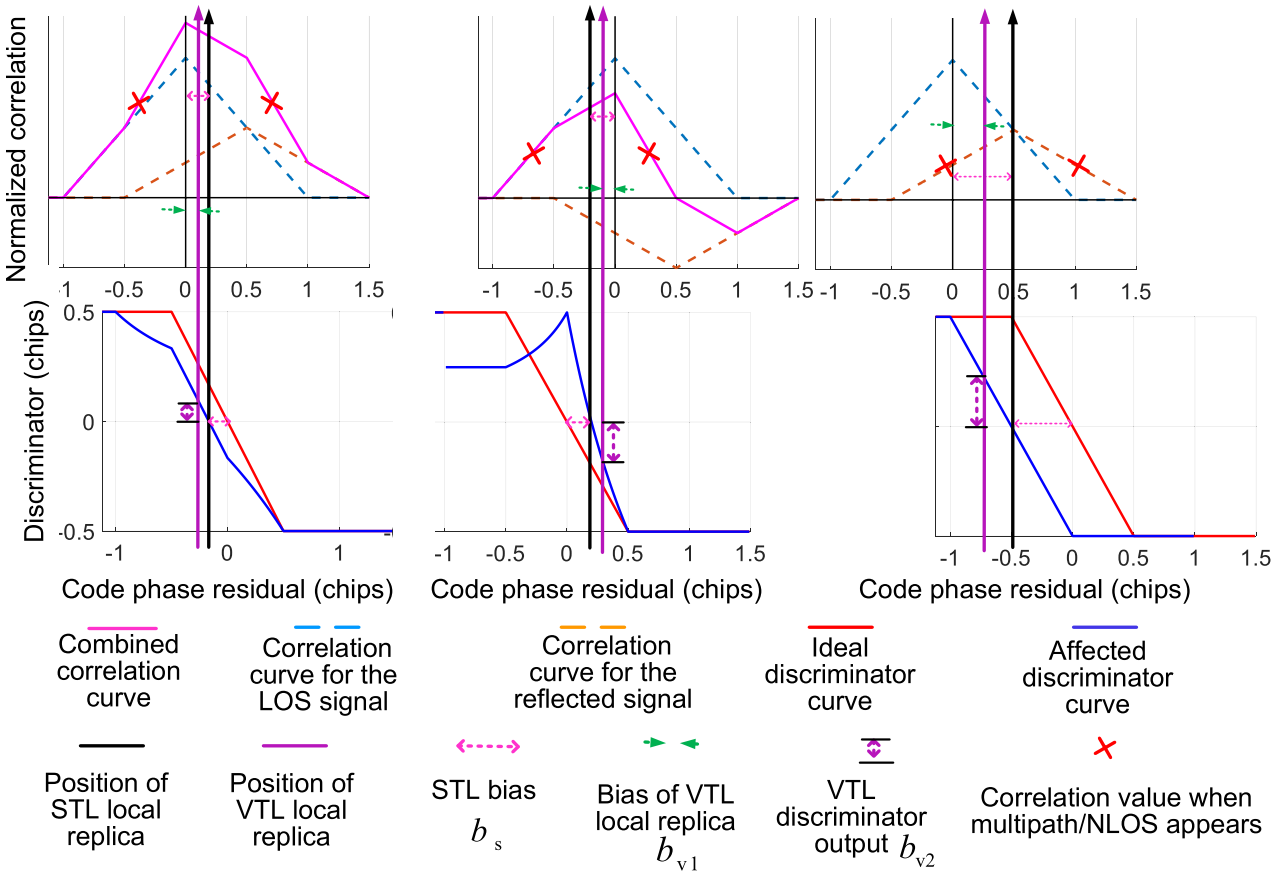

Fig. 3 Comparison of the multipath/NLOS induced bias for Early minus Late correlator spacing of 1 chip. The top panels are the correlation curves, while the bottom ones are the corresponding discriminate curves. The three panels from left to right are the results of constructive multipath, destructive multipath, and NLOS

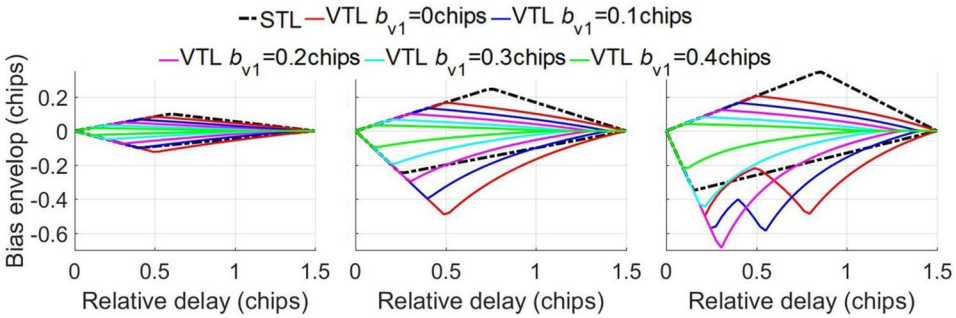

Fig. 4 Multipath induced bias envelop for Early minus Late correlator spacing of 1 chip. The dashed line denotes the multipath bias envelop of a STL. The solid curves denote the multipath bias envelop given a different offset of the local replica. The amplitude ratios of the reflected signal to the LOS one from left to right are $\alpha = 0.2, \alpha = 0.5, \alpha = 0.7$

bias envelop for a specific local replica offset. Hence the VTL plots in Fig. 4 are no longer a multipath bias envelop in the traditional sense. The multiple VTL plots are given here more to reveal the fact that multipath induced bias to a VTL in some cases is not smaller than to an STL, which can be seen from the destructive multipath situation for certain values of b_{v1} and α in Fig. 4.

Tracking bias propagation

To illustrate the bias propagation in a VTL, the biased measurement residuals are represented by

$$\tilde{\mathbf{z}}_k = \mathbf{H}_k \delta \mathbf{x}_k + \mathbf{b}_k + \mathbf{n}_k \tag{29}$$

Zero elements of the bias vector $\mathbf{b}_k$ denote the bias free channel, while the nonzero elements stand for the corresponding

bias value. The posterior user state residual estimation can be represented by

$$\delta\tilde{\mathbf{x}}_k^+ = \mathbf{K}_k\tilde{\mathbf{z}}_k = \mathbf{K}_k\left(\mathbf{H}_k\delta\mathbf{x}_k + \mathbf{n}_k\right) + \mathbf{K}_k\mathbf{b}_k \tag{30}$$

where $\mathbf{K}_k$ denotes the EKF gain matrix (Xu et al. 2020). The last term in (30) is the bias effect on the user state residual estimation. The user state after the update is denoted as $\tilde{\mathbf{x}}_k^+$, which is used to predicate the user state in the next epoch by

$$\begin{aligned}\tilde{\mathbf{x}}_{k+1}^- &= \mathbf{F}_{k,k+1}\tilde{\mathbf{x}}_k^+ = \mathbf{F}_{k,k+1}\left(\mathbf{x}_k^- + \delta\tilde{\mathbf{x}}_k^+\right)\\ &= \mathbf{F}_{k,k+1}\left(\mathbf{x}_k^- + \delta\mathbf{x}_k^+ + \mathbf{K}_k\mathbf{b}_k\right)\end{aligned} \tag{31}$$

The above a prior predicated user state is used to calculate the synchronization parameters of the local replica in the following epoch, which is different from the ones calculated by the user state without bias. The difference between the biased synchronization parameters and normal ones is below

$$\begin{aligned}\begin{bmatrix}\Delta\tilde{\boldsymbol{\tau}}_{k+1}^-\\ \Delta\tilde{\mathbf{f}}_{d,k+1}^-\end{bmatrix} &= g^{-1}\left(h\left(\tilde{\mathbf{x}}_{k+1}^-\right)\right) - g^{-1}\left(h\left(\mathbf{x}_{k+1}^-\right)\right)\\ &= \bar{g}^{-1}\left(\mathbf{H}_k\left(\mathbf{F}_{k,k+1}\mathbf{K}_k\mathbf{b}_k\right)\right)\end{aligned} \tag{32}$$

The product $\mathbf{H}_k\mathbf{F}_{k,k+1}\mathbf{K}_k$ is a non-diagonal matrix, hence the elements in the above difference vector are nonzero for all the tracking channels. The difference vector in (32) is termed the propagated tracking bias, for it originates from the tracking bias in the channel with multipath/NLOS reception propagating to all the other tracking channels.

Experiment results

It is known that the performance of an STL depends on its loop parameters, while only one set of parameters is chosen in our experiments to obtain some sample results to illustrate the different characteristics between STL and VTL. For different application requirements, corresponding results can be obtained by the proposed semi-analytic model using different parameter configurations.

Sample results from the proposed semi-analytic model

In the following results, a second-order loop filter with a bandwidth of 10 Hz is used for PLL and 2 Hz for DLL in the STL. The ECEF coordinate system user state is initialized as $\mathbf{x}_0 = \left[p_{x0}, p_{y0}, p_{z0}, v_{x0}, v_{y0}, v_{z0}, \mathrm{c}t_{b0}, \mathrm{c}\dot{t}_{b0}\right] = [0, 0, 0, 50, 10, 0, 0, 0]$, and 6 satellites are assumed to be visible, with the sky view shown in Fig. 5. The $\mathrm{C/N_0}$ of the 6 satellite signals are all 45 dB-Hz. One reflected signal of SV1 is simulated with an extra delay of 0.5 chips relative to the LOS signal, the amplitude of the reflected signal is half of the LOS one. The carrier frequency remains the same with the LOS signal. The multipath-induced tracking bias reaches its positive maximum when the carrier phase difference between the reflected signal and the LOS signal is zero and reaches its negative maximum when the carrier phase difference is π. Therefore, the phase difference is set to a fixed value of zero to obtain the bias envelop of the constructive multipath case, which is set to a fixed value π to get the bias envelop of the destructive multipath case. The Early-minus-Late correlator spacing used in the following simulations is 1 code chip.

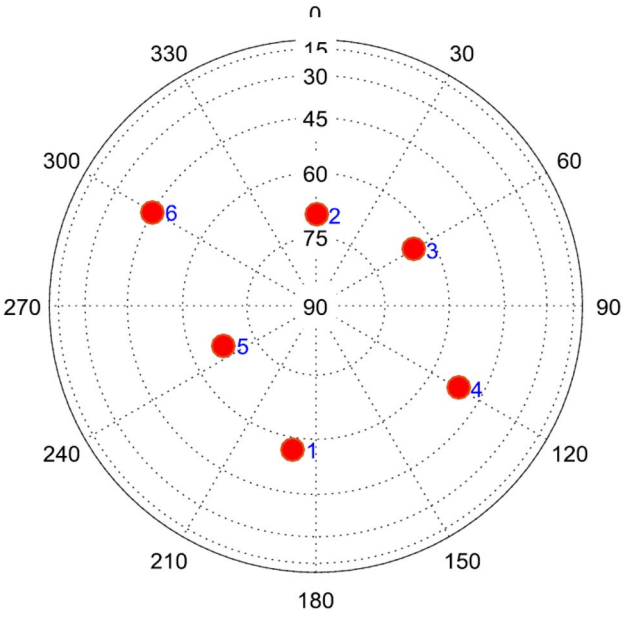

Fig. 5 Sky view used in the simulation. The red circles denote the satellites with the number next to them denoting the PRN index

Figure 6 gives the experiment results as the relative code delay between the reflected signal and the LOS signal varies from 0 to 1.5 chips in a constructive multipath test case. The mean value in the multipath duration period is given for each relative code delay. Therefore, the overall tracking bias between the STL and the VTL can be compared for each relative code delay of multipath. It is noted that the VTL tracking bias in the SV1 channel is smaller than that of the STL for all relative code delay. The MSE of the horizontal positioning result on the bottom panel shows when the relative code delay is less than half a chip, the positioning performance of STL and VTL are similar, while the VTL is superior as the relative code delay increases.

Figure 7 gives the experiment results of the mean values in a destructive multipath situation. It is noted that the positioning performance of the STL is superior as the relative code delay exceeds about 0.2 chips. It should be pointed out that it is still not proper to conclude that a VTL is inferior to an STL in a destructive multipath situation because an STL

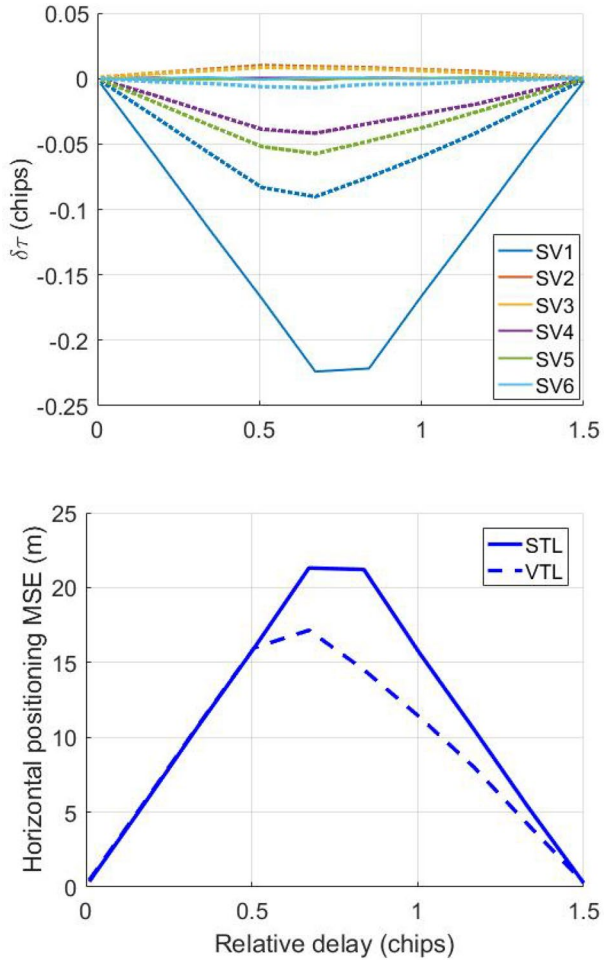

Fig. 6 Comparison of STL and VTL in a constructive multipath situation. The solid lines are from the STL, while the dashed ones are from the VTL. The mean values of the true code phase residuals are shown on the top panel, with colors denoting the results from different channels. The MSE for horizontal positioning is shown on the bottom panel

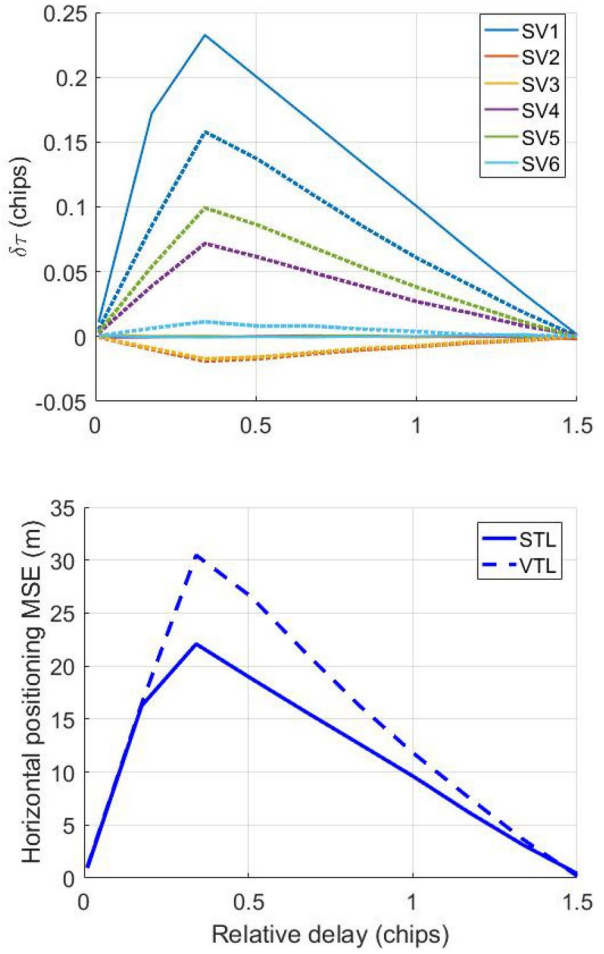

Fig. 7 Comparison of STL and VTL in a destructive multipath situation. The solid lines are from the STL, while the dashed ones are from the VTL. The mean values of the true code phase residuals are shown on the top panel, with colors denoting the results from different channels. The MSE for horizontal positioning is shown on the bottom panel

might lose lock and need to re-acquire the satellite signal when the signal recovers. However, the loss of lock of a satellite signal in the VTL does not require the re-acquisition of the signal for the internal aiding of VTL. This superiority of a VTL is extremely important in situations with limited in-view satellites.

Figure 8 shows the experimental results in a NLOS situation as the relative code delay varies. It is noted from the top left panel that the biased value of the STL is linearly related to the relative code delay when the relative code delay is less than about 1.4 chips. The bias value decreases as the relative code delay further increases because it exceeds the linear extents of the discriminator. The positioning MSE on the bottom panel of Fig. 8 shows that the positioning performance of the VTL is superior as the relative code delay increases.

Verification of the semi-analytic model

The effectiveness of the proposed semi-analytic model is also verified by the comparison between its outputs and the results from the SDR by processing simulated data with the same configuration. Since the coherent integration period of the SDR is 1 ms, we use 1 ms coherent integration period in the semi-analytic model in this experiment. To show the effect more clearly, the C/N0 of all the satellite signals under tracking is set to 53 dB-Hz. One reflected signal of SV2 is simulated with an extra delay of 0.5 chips relative to the LOS signal, and the amplitude of the reflected signal is half of the LOS one. The results of the NLOS situation are given in Fig. 9. It is noted that the STL results of both the semi-analytic model and the SDR show a sharp value when the NLOS appears, while they also show an opposite sharp value as the multipath

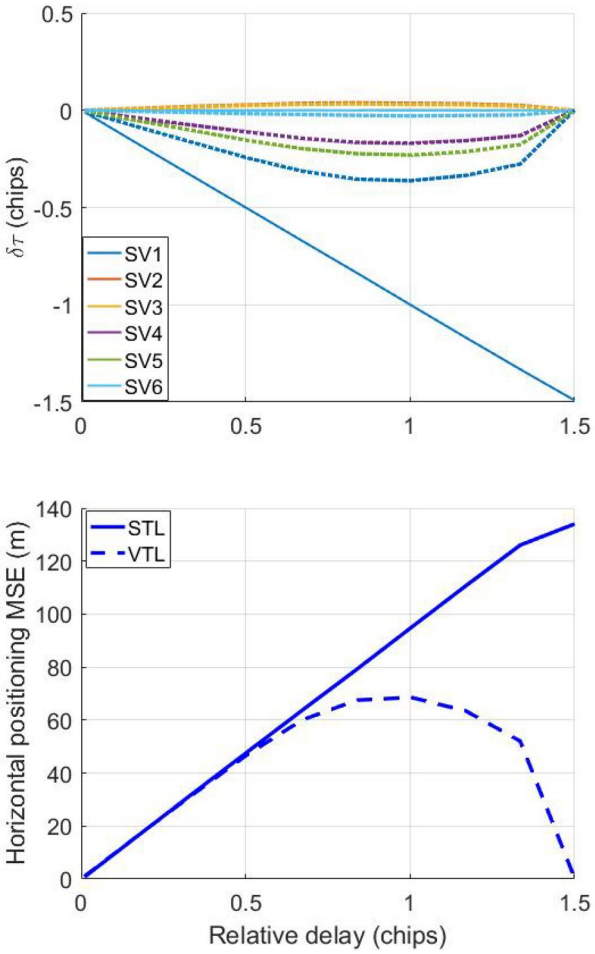

Fig. 8 Comparison of STL and VTL in NLOS situation. The solid lines are from the STL, while the dashed ones are from the VTL. The mean values of the true code phase residuals are shown on the top panel, with colors denoting the results from different channels. The MSE for horizontal positioning is shown on the bottom panel

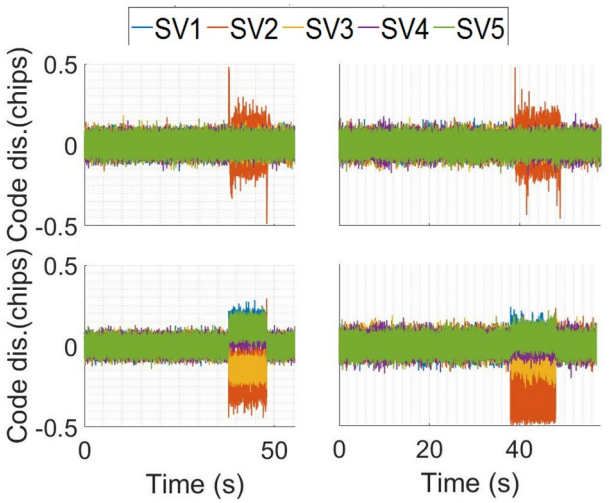

Fig. 9 Code discriminator output comparison between the semi-analytic model and the simulated data processed by the SDR in an NLOS situation. Different colored lines in each figure indicate the results from different tracking channels. The panels are the results from the STL semi-analytic model (top left), the STL SDR (top right), the VTL semi-analytic model (bottom left), and the VTL SDR (bottom right)

disappears. During the NLOS period, the discriminators output smaller values because the delay lock loop locked onto the reflected signal. The consistent can also be noted in the VTL results, where both of the results show a similar bias propagation phenomenon. The results for the multipath situation also show high similarities, which are not given here.

Conclusions

A semi-analytic model with a uniform framework is proposed to analyze and compare the performance of an STL and VTL efficiently and effectively. The signal quality information can be incorporated directly for multipath and NLOS configurations, allowing for evaluate the performance in different multipath/NLOS situations. Robustness of the STL and VTL to Multipath and NLOS reception is given, including the multipath induced bias envelop. To verify the analysis, we give sample results from the proposed model. The tracking results from an SDR with simulated NLOS data show high similarity with the results of the proposed semi-analytic model.

Motivated by the interesting results that STL performance outperforms VTL in a certain destructive multipath situation, the relationship between the multipath or NLOS parameters and their induced tracking bias to VTL will be analyzed in our future work.

Acknowledgements This work is supported by the Scientific Research Program of Tianjin Municipal Education Commission (2021KJ042) and the Project of the Natural Science Foundation of Tianjin (19JCQNJC01000).

Data availability The involved simulated data is available by email from the corresponding author.

References

Bhattacharyya S (2018) Vector loop transfer functions and noise bandwidths. Navigation 65(1):55–72

Bhattacharyya S, Demoz GE (2010) Development and validation of parametric models for vector tracking loops. Navigation 57(4):275–295. https://doi.org/10.1002/j.2161-4296.2010.tb01783.x

Borio D, Anantharamu PB, Lachapelle G (2011) SATLSim: a semi-analytic framework for fast GNSS tracking loop simulations. GPS Solut 15(4):427–431. https://doi.org/10.1007/s10291-011-0221-0

Hsu LT (2018) Analysis and modeling GPS NLOS effect in highly urbanized area. GPS Solut 22(7):1–12

Hsu LT, Jan SS, Groves PD, Kubo N (2015) Multipath mitigation and NLOS detection using vector tracking in urban environments. GPS Solut 19(2):249–262. https://doi.org/10.1007/s10291-014-0384-6

Spilker JJ (1996) Global positioning system: theory and application. Fundamentals of signal tracking theory. American Institute of Aeronautics, Washington

Jia QQ, Wu RB (2020) A uniform framework semi-analytic model for STL and VTL performance evaluation. Proc: ION GNSS+ 2020, Institute of Navigation, Virtual, Sept 21–25, 3108–3119. https://doi.org/10.33012/2020.17706

Jia QQ, Wu RB, Wang WY, Lu D, Wang L, Li J (2017) Multipath interference mitigation in GNSS via WRELAX. GPS Solut 21(2):487–498. https://doi.org/10.1007/s10291-016-0538-9

Kaplan ED, Hegarty C (2006) Understanding GPS. Principles and applications. 2nd ed. Artech House, Boston

Lashley M, Bevly DM, Hung JY (2009) Performance analysis of vector tracking algorithms for weak GPS signals in high dynamics. IEEE J Sel Top Signal Process 3(4):661–673. https://doi.org/10.1109/JSTSP.2009.2023341

Julien L, Thierry R, Mohamed S, Jean-Yves T, Willy V (2019) Multipath mitigation for GNSS positioning in an urban environment using sparse estimation. IEEE Trans Intell Transp Syst 20(4):1316–1328. https://doi.org/10.1109/TITS.2018.2848461

Luo, ZB, Zhao L, Ding JC, Wu MY (2019) Tracking error analysis and performance evaluation method for GNSS non-coherent vector tracking loop. Proc: CSNC 2019, Springer Nature Singapore Pte Ltd, Beijing, China, May 21–23, 450–462

Lashley M (2009) Modeling and performance analysis of GPS vector tracking algorithms, 2009. Dissertation, Auburn University, Alabama

Nee RDJV (1992) Multipath effects on GPS code phase measurements. Navigation 39(2):177–190. https://doi.org/10.1002/j.2161-4296.1992.tb01873.x

Xu B, Hsu LT (2019) Open-source MATLAB code for GPS vector tracking on a software-defined receiver. GPS Solut 23(2):275. https://doi.org/10.1007/s10291-019-0839-x

Xu B, Jia QQ, Hsu LT (2020) Vector tracking loop-based GNSS NLOS detection and correction: algorithm design and performance analysis. IEEE Trans Instrum Meas 69(7):4604–4619. https://doi.org/10.1109/TIM.2019.2950578

Zhao SH, Lu MQ, Feng ZM (2011) Implementation and performance assessment of a vector tracking method based on a software GPS receiver. J Navigation 64(S1):S151–S161. https://doi.org/10.1017/S0373463311000440

Zhang GH, Xu B, Ng HF, Hsu LT (2020) GNSS RUMS: GNSS realistic urban multi-agent simulator for collaborative positioning research. Remote Sens 13:544

Qiongqiong Jia received her M.Sc. in Communications Engineering from the Civil Aviation University of China (CAUC) in 2011. She also received an advanced master's degree in Air Navigation Engineering from École Nationale de l'Aviation Civil in 2015. She is an associate professor with the CAUC. Her research interests include adaptive signal processing for multipath, NLOS and interference mitigation in GNSS.

Li-Ta Hsu received a Ph.D. degree in aeronautics and astronautics from National Cheng Kung University, Taiwan, in 2013. He is currently an associate professor with the AAE, The Hong Kong Polytechnic University. He is an associate fellow in the royal institute of navigation (RIN) and a council member of the institute of navigation (ION) since 2019. His research interests include GNSS positioning in challenging environments and localization for autonomous and unmanned aerial vehicles.

Renbiao Wu received a Ph.D. degree from Xidian University, Xi'an, China, in 1994, in electrical engineering. Since January 1999, he has been in the Tianjin Key Laboratory for Advanced Signal Processing, CAUC, where he is currently a Chaired Professor and the Director of the laboratory.